Wake Vortex Tangential Velocity Adaptive Spectral (TVAS) Algorithm for Pulsed Lidar Systems

Hadi S. Wassaf
John A. Volpe National Transportation Systems Center, Cambridge MA, USA
hadi.wassaf@dot.gov

David C. Burnham
Scientific & Engineering Solutions Inc., Orleans MA, USA
dcburnham@scensi.com

Frank Y. Wang
John A. Volpe National Transportation Systems Center, Cambridge MA, USA
frank.wang@dot.gov

1. Introduction

Doppler Lidars have proven to be a major enabling technology for measuring aircraft wake vortices and affecting safety and capacity changes over the past decades[1,2,3]. Doppler Lidars have two forms, namely, continuous-wave (CW) and pulsed. CW Lidars were first used to measure wakes in the 1970s and generated useful data on wake decay[4,5,6]. They provide good spatial resolution up to a range on the order of 150 m beyond which this resolution is lost due to the limitation on the size of the focusing optics. In the late 1990s, commercially available coherent pulsed Lidars were developed and achieve range resolution directly via range gates, which permit wake measurements over distances of several kilometres. This development of increased measurement range coincided with the resurgence of interest of the wake community in quantifying wake hazards in parallel runway operations, as well as in vortices generated at altitudes greater than 1000 feet. As such pulsed Lidars became the preferred technology for wake vortex data collection. This data is used for safely changing and establishing wake turbulence standards and procedural developments [1,7,8].

To date, the Lockheed Martin Coherent Technologies (LMCT) matched-filter software[9] is the only commercially available pulsed Lidar wake vortex processing package and has provided the bulk of the wake data used by the Federal Aviation Administration (FAA) and EUROCONTROL to change wake separation rules. The need to have an alternative is mainly motivated by the following 3 points:

a- Common to many engineering disciplines, a less conservative procedure can be designed safely only by reducing the data measurement uncertainty.
b- For outlier analysis of wake vortex studies, it is highly desirable to have more than one algorithm to perform cross checks in order to ensure the observations are not dominated by processing artefacts.
c- Future processing needs of the Federal Aviation Administration (FAA) require the flexibility and the capability to use Lidars from other manufacturers.

In 2008 the FAA tasked the Volpe Center with the development of a government owned processing package capable of performing wake detection, characterization and tracking. The current paper presents the background, progress, and capabilities to date on the Volpe Center developed Tangential Velocity Adaptive Spectral (TVAS) wake processing package. Since TVAS is intended to supplement rather than duplicate the LMCT processing, the decision was made to use the influential work of the German Aerospace Center (DLR)[10,11] as the baseline and supplement it with additional enhancements.

The TVAS wake processing package is comprised of four major components:

1. Detection.
2. Localization.
3. Circulation Estimation.
4. Kalman Filter (KF) based automated tracking.

With the exception of automated tracking, the details of these components are discussed later in this paper. A brief theoretical background is first provided, the details of the

algorithm components are subsequently described in terms of differences and enhancements over the DLR algorithms. Finally, A simulation based validation along with cross-validation of TVAS against the LMCT processing package applied to real Lidar data is presented.

The KF tracker is still not fully validated. Its automation capability tested successfully in simulations, and is user assisted when processing field data. The development, tuning, and validation of the KF for full automation will be the subject of future publications.

2. Brief Theoretical Background

The range resolution of a pulsed Lidar is significantly less than that of a typical CW Lidar and is comparable to the size of wake vortex structures. Therefore TVAS, DLR and LMCT processing algorithms, as well as the numerical simulations of the pulsed Lidar signal require an analytical model that describes how the characteristics of the measured averaged spectrum are influenced by the flow field and the Lidar response. In the case of TVAS, an estimate of the model spectrum based on the locations of the vortices and initial measurements of their corresponding strengths is needed to further refine the circulation measurements (discussed later in this paper). The LMCT maximum likelihood processing algorithm also requires a model spectrum to be used in the calculation of the optimal matched filters. The spectral model used by TVAS for the case of a rectangular FFT window is shown in equation (1)

$$\hat{S}_{nz}(f) = B.SNR(z_o)\int_{-\infty}^{\infty} Q'(z).e^{-\frac{1}{2}\frac{\left(f+\frac{2}{\lambda}V_r(z)\right)^2}{\sigma_{fb}^2}}dz + 1 \qquad (1)$$

With $\sigma_{fb} = \sqrt{\sigma_f^2 + \left(\frac{1}{3T}\right)^2}$ (2)

T is the duration of the FFT window.

$$\boldsymbol{\sigma_f = \frac{1}{4\pi\sigma}} \qquad (3)$$

Where $\boldsymbol{\sigma}$ represents the width of the Gaussian pulse. $V_r(z)$ is the line of site (LOS) component of the flow field at the radial distance z from the transceiver.Q'(z) is a function defining the RG resolution.

$$Q'(z) = \frac{2\sqrt{2\pi}\sigma}{cT}\left\{\begin{array}{c}\mathrm{erf}\left(2\frac{z_0-z}{\sqrt{2}c\sigma}+\frac{T}{2\sqrt{2}\sigma}\right)\\ \mathrm{erf}\left(2\frac{z_0-z}{\sqrt{2}c\sigma}-\frac{T}{2\sqrt{2}\sigma}\right)\end{array}\right\} \qquad (4)$$

The detailed derivation of this model along with the definition of the various parameters is presented in Appendix A.

For the purpose of the refinement of the circulation estimates (discussed in the next section) TVAS calculates the spectral model using a numerical implementation of eq. (1).

3. TVAS Algorithm Description

As mentioned earlier in this paper the overall flow of the algorithm is similar to that of the DLR algorithm[10] with additional enhancements. This section provides a description of the enhancements.

a. Detection

The wake detection is performed by calculating the ratio of the average spectral width in a predefined approach corridor to that of the background. This is tuned based on statistics of this ratio over an observation period when no wakes are present, and setting the threshold so that probability of false alarm $P_{FA}=10^{-3\sim-4}$. This approach has proven to be robust for identifying the start of a flyby for Medium ICAO wake class aircraft and larger.

b. Localization

The location of the wake is determined as the mean between the peak velocities above and below the core. The determination of the vortex induced velocities requires the important step of calculating the envelope velocities[10,11]. This is done by applying a threshold to the measured spectrum associated with each range gate and extracting the negative and positive velocities at the intersections as illustrated in the following figure.

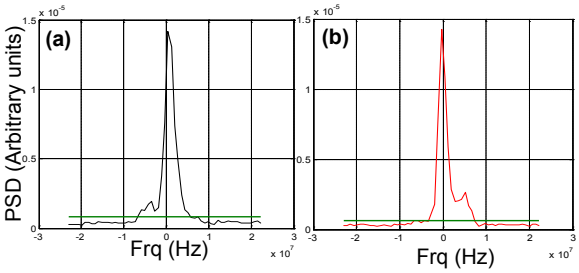

Fig. 1: Extraction of envelope velocities: Spectra corresponding to an RG above (a), and below (b) the P-vortex. The 2 intersections with the threshold (green) are the envelope velocities for each RG.

The validity of this approach is based on the premise that vortex induced velocities are added perturbations over the background wind and will produce the largest velocities observed within a scan. Moreover, there is a distinct flow pattern associated with the vortex perturbed wind field. Therefore, despite the large size of a range gate the vortex induced velocities can be discerned from the background by considering the spectral region outside the background velocities represented by the main lobe in the spectrum acting as a clutter region. This technique falls under the Spectral Time Adaptive Processing (STAP) in the field of radar signal processing. Due to the scan-to-scan as well as within-scan fluctuations in SNR, a static threshold may

produce inconsistent results. In addition the threshold should be low enough to detect weak spectral peaks corresponding to large velocities but still above the variability of the noise floor (i.e. requiring a very low probability of false detection). Therefore, TVAS uses a dynamic threshold that adapts to the SNR for each RG. It can be seen from equation (1) that the PSD value corresponding to a particular velocity is a function of SNR. For an RG located at (R, ϕ),The following form of the threshold was used

$$T(R,\phi) = k.\widehat{N}.\frac{SNR(R,\phi)}{SNR_o} \quad (5)$$

Where $\widehat{N}$ is the estimate of the average Noise PSD outside the signal region of the spectrum. $SNR(R,\phi)$is the calculated SNR for this RG. SNR_0 is the average SNR for the current scan.

The center of each vortex is taken to be the mid point between the most positive and most negative velocity along the range to the vortex. TVAS achieves this localization process by employing image processing techniques to segment out the regions that are associated with high induced velocities and consider all possible negative and positive envelope regions associations. The association that is most consistent with a vortex flow is selected. This process identifies two valid peaks for each vortex even when peaks from the two vortices overlap. This approach proved to be robust in the early stage of the vortex decay when both vortices are present. For the subsequent scans a state of the art Kalman Filter (KF) is used to predict the search region locations for each of the 2 envelope peaks associated with a particular vortex. For the field data presented in this paper, the peak search regions predicted by the KF are manually inspected and corrected. In its current form, the KF rate of successful predictions was better than 80% for field data and 100% for simulated data.

c. Circulation Estimation Enhancements

After the vortex location is found the last step is to estimate the circulation strength. This estimation is done in two iterations. The first iteration uses the velocity envelopes to obtain an initial estimate of the circulation. The second step is a refinement step and is used to improve the initial estimate. Both iterations consider the RGs at distance of 5 to 15 meters on either side of the core (fixed R, varying ϕ). The refinement step uses the initial circulation to estimate the spectral model using equation (1) for each of the RGs of interest. A refined floating threshold (FT) is then estimated[11] to obtain refined envelope velocities that lead to an improved circulation measurement. TVAS adds 3 sets of enhancements to this baseline algorithm.

The first set of enhancements is geared toward obtaining a more representative spectral model. First, as vortices near the ground, a 4 vortex model that considers the image vortices is used to calculate this model. This is done to better emulate the vortex flow modification due to the ground imposed boundary condition. Second, a statistical analysis of the measured spectra in the wake-free region is used to obtain a spectral width consistent with the background turbulence. The spectral modelling uses this width instead of the nominal spectral width of the monitor pulse spectrum. Finally, the spectral model uses a more realistic Burnham-Hallock (BH) instead of the Lamb-Oseen model in the calculation of circulation. The choice of the model is however user selectable.

The second set of enhancements is focused on a better use of the spectral model in refining the estimated tangential velocities. In particular, it addresses the following deficiency in the FT algorithm. When attempting to estimate low velocities close or inside the main spectral lobe, the FT algorithm tends to over estimate the velocities and therefore introduces a bias in the circulation estimates. To address this issue a minimum mean square error (MMSE) algorithm is used when FT produces velocities on the order of the spectral width or smaller. The MMSE algorithm first calculates the error between the spectral model and measured spectrum for the same RG.

$$MSE(\Gamma_w) = \int_{f_i}^{f_f} \left(\hat{S}_{nz}(f|x_w, z_w, \Gamma_w) - S_{nz}(f) \right)^2 df \quad (6)$$

Where x_w and z_w represent the lateral and vertical position of the vortex's center respectively.
The circulation Γ_w is the one that minimizes the MSE.

$$\Gamma_{MMSE} = Argmin_{\Gamma_w}\{MSE(\Gamma_w)\} \quad (7)$$

Since the FT algorithm is faster and produces accurate results for estimating moderate to large velocities, the MMSE algorithm is activated only when the FT algorithm produces small velocities. The result is a hybrid algorithm.

The third and last set of enhancements is geared towards guarding against outliers from the hybrid algorithm. Despite the added robustness of the hybrid algorithm over the baseline FT algorithm it is possible at times that an incorrect spectral model can result in a large error in circulation estimate and that an alternative simpler algorithm might produce

better results. To guard against these outliers two additional circulation estimates are considered. The selection of the appropriate algorithm is done automatically and objectively by considering the differences between these results and a smoothing spline curve applied to the hybrid circulation results. This smoothed curve is used only as an arbitrator between the circulation values provided by the 3 algorithms. The 3 circulation algorithms that enter the arbitration process at each step are:

a- **Envelope**: The envelope velocities (described in the localization section) corresponding to RGs between d_{min} to d_{max} above and below the core (nominally d_{min}=5 to d_{max}=15 meters) are used to estimate total circulation.

b- **Peak velocity**: The peak velocities above and below the core are only used in conjunction with the separation between those peaks are used to estimate the circulation.

c- **FT/MMSE hybrid:** The main circulation algorithm for TVAS and was described in the second set of enhancements.

Finally, it is worthy to note that the model used by TVAS to calculate total circulation, as well as, the choice of d_{min} and d_{max} are user selectable. In particular, the choice of a point vortex model with d_{min}=5 (m) and d_{max}=15 (m) results in what is commonly referred to as the 5-15 (m) circulation. Because of the potentially superior performance of MMSE in the case of low velocities, the range of distances from the core that are used for analyzing field data presented in later in this paper is extended to d_{min}=3 (m) and d_{max}=17 (m) in conjunction with BH vortex model.

4. TVAS Validation

The TVAS processing package was validated via simulation as well as field data collected in an airport environment. The simulation provides a known reference to quantify the errors and evaluate the improvements provided by the hybrid algorithm under pristine conditions. For the field data, no such known reference exist, and the validation is performed in the form of a comparison with the commercially available LMCT algorithm. The simulation SNR was set to 5 dB. This is near the lower limit of acceptable SNR for field data. The field data had good SNR on the order of 10 dB. The SNR is calculated over the 7.8 Mhz band centered at the zero Doppler frequency (consistent with the LMCT definition of SNR).

a. Simulation Results

A Lidar data simulator developed by Volpe was used to generate the averaged spectra for each scan. The input to the simulation consisted of the BH representation of a B747-400 wake generated at an altitude of 79.3 meters (260 feet) and approximately 2 km away from the Lidar. A crosswind of 1 m/s was also included in the simulation. The scan duration is approximately 7.5 seconds and simulation time is 220 seconds. The following figure shows the input reference tracks together with the results of the TVAS processing package.

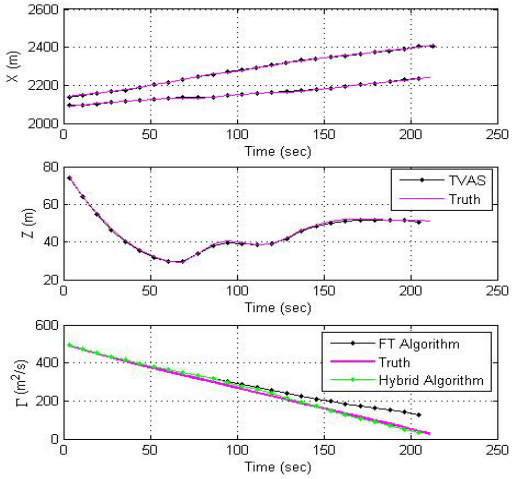

Fig. 2: Simulation input together with the measured tracks using the TVAS wake processing package. X is the lateral position with the positive direction being away from the Lidar. Z is altitude above ground.

These results show that TVAS position estimates are quiet accurate. The results also show that both the hybrid and the FT circulation estimation methods perform well for high circulations with the hybrid method outperforming the FT for low circulations. This is expected because low circulations produce velocities closer to the main spectral lobe where the FT algorithm introduces an upward bias on the results. These observations are clearly supported by the tabular error results shown below

Simulation	Mean	Standard deviation
$X_{TVAS} - X_{True}$	-0.22 (m)	2.37 (m)
$Z_{TVAS} - Z_{True}$	-0.69 (m)	1.38 (m)
$\Gamma_{FT} - \Gamma_{True}$	31.27 (m^2/s)	25.53 (m^2/s)
$\Gamma_{Hybrid} - \Gamma_{True}$	4.87 (m^2/s)	8.34 (m^2/s)

Table-1: Statistical error analysis on the simulated data

b. Field Data Results

The second part of the validation is based on Field data. Lidar data collected using LMCT hardware from 3 passages of a reference aircraft through the Lidar scanning plane were analyzed using TVAS as well as LMCT wake processing packages. The TVAS enhanced circulation algorithm was used to estimate the circulation values. The data was first

normalized, and the non-dimensional positions and circulations from both algorithms are presented in scatter plots shown in figure 3 below.

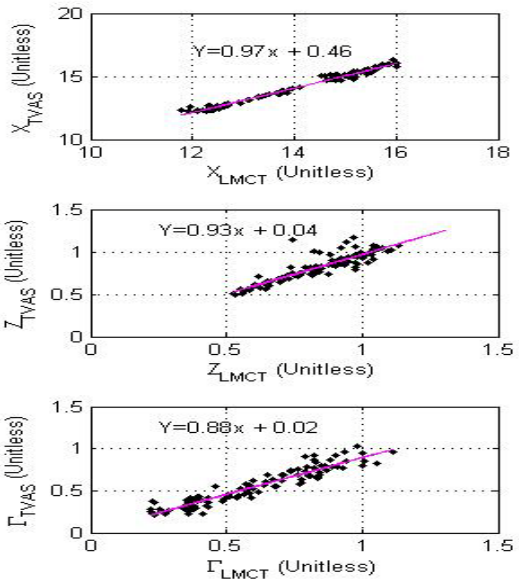

Fig. 3: Scatter plots of TVAS non-dimensional positional and circulation results versus those outputted by the LMCT algorithm for 3 wake tracks from a reference aircraft. The equation of the linear regression lines are shown on each of the 3 graphs

These results show good agreement between the LMCT and TVAS outputs with the TVAS circulation results being slightly lower than those of LMCT. Both TVAS and LMCT calculate total circulation. The TVAS total circulation is based on BH model fit to the velocity measurements refined by the hybrid algorithm. LMCT matched filters are also calculated based on the BH vortex model. The source of this discrepancy is subject to investigation. However, a statistical analysis of the difference between the two algorithms reveals that this bias is only on the order of 4% to 7% of initial circulation. The standard deviation of the difference is on the order of 7.6% as seen in the table below.

N-Vortex	Mean	Std
$(\Gamma_{TVAS} - \Gamma_{LMCT})/\Gamma_o$	4.3 e-2	7.6 e-2
$(X_{TVAS} - X_{LMCT})/b_o$	3.7 e-2	17 e-2
$(Z_{TVAS} - Z_{LMCT})/b_o$	-2.6 e-2	8 e-2

(a)

P-Vortex	Mean	Std
$(\Gamma_{TVAS} - \Gamma_{LMCT})/\Gamma_o$	-7.1 e-2	7.3 e-2
$(X_{TVAS} - X_{LMCT})/b_o$	7.2 e-2	15.4 e-2
$(Z_{TVAS} - Z_{LMCT})/b_o$	-2.61 e-2	11.9 e-2

(b)

Table-2: Statistical results from the analysis of the difference between LMCT and TVAS processing packages. (a) N-Vortex (furthest from Lidar and negative circulation). (b) P-Vortex (closest to Lidar (+) circulation).

An analysis of the self consistency of circulation measurements within each of the two processing packages is subsequently performed. This is done by taking the mean normalized circulation decay $<\Gamma(t)>$ of the 3 tracks and then calculating the standard deviation of the differences between all three decay curves and this mean decay curve for each of the two algorithms $std(\Gamma(t)-<\Gamma(t)>)$.

$std(\Gamma_{TVAS}(t) - <\Gamma_{TVAS}(t)>)/\Gamma_o$	3.8 e-2
$std(\Gamma_{LMCT}(t) - <\Gamma_{LMCT}(t)>)/\Gamma_o$	6.5 e-2

Table-3: Self consistency tabular results for each of the TVAS and LMCT processing packages

The differences between the two algorithms (Table-2) are on the order of the inconsistencies within either of the two algorithms (Table-3). Therefore these differences are not very significant. However, as mentioned earlier in this section, further investigations will be carried out in order to resolve the sources of these differences. It is also worthy to note, that although Table-3 seems to indicate that the TVAS results are slightly more consistent than the LMCT algorithm. This difference is likely related to the lack of circulation smoothing by LMCT and the third set of enhancements described in the circulation estimation section that bound the variability in TVAS circulation estimates. Furthermore, a much larger statistical set than the currently used 3 tracks is needed for more conclusive self-consistency results

4. Conclusion

The TVAS processing package for the tracking and characterization of wake vortices using pulsed Doppler Lidar systems was presented. The published DLR algorithms for localization and circulation estimation formed the starting point for this development. The enhancements provided by TVAS in the areas of spectral modelling, localization and circulation estimations were described. Finally, simulation and field data validation of TVAS were presented. The simulation results showed that the hybrid algorithm is significantly less biased than the DLR FT algorithm at low circulations and produces a better match relative to the known input circulation values. In the case of field data, the differences between the TVAS and LMCT results were on the order of the self consistency within each algorithm and are therefore not very significant. Although the discrepancy is not believed to be important in certain applications of the data, the sources of differences will be the subject of future studies. A KF tracker based on wake vortex dynamics is undergoing tuning and validation for the purpose of full automation of the processing, and will be presented in future publications.

4. Acknowledgements

The authors would like to thank Steve Lang and Jeff Tittsworth of the FAA Wake Turbulence Program for their continued support of this development. We also acknowledge the support from Lockheed Martin Coherent Technologies for providing additional details on the WindTracer system.

.

5. References

1. "The National Rule Change (NRC) 1.5-Nautical Mile Dependent Approaches to Parallel Runways Spaced Less Than 2,500 Feet Apart", FAA ORDER JO 7110.308, Change 2, U.S. Department of Transportation, Federal Aviation Administration, (September 2010)
2. "Aircraft Information Fixed-Wing Aircraft", FAA N JO 7110.525, Appendix A, U.S. Department of Transportation, Federal Aviation Administration, (April 2010)
3. "The Design of the A380 Wake Vortex Separation", ICAO State Letter TEC/OPS/SEP – 08-0294.SLG, (2006)
4. S. Winkler and G. Perras, "An Analysis of Wake Vortex Lidar Measurements at LaGuardia Airport", MIT Lincoln Laboratory Report ATC-318, 2004
5. R. M. Heinrichs et al, "Analysis of Circulation Data from a Wake Vortex Lidar", 35th Aerospace Sciences Meeting & Exhibit, Reno, NV, AIAA 97-0059, (Jan 1997).
6. S. A. Teager et al., "Flight Test Investigation of Rotorcraft Wake Vortices In Forward Flight", DOT/FAA/CT-94/117, FAA Technical Center, Atlantic City Airport, NJ (February 1996),
7. "WIDAO project in Paris Charles de Gaulle airport; Procedure changes", Ref-09/050 / DCS/ANA/SMN, (April 2009).
8. K. Dengler et al., "Crosswind thresholds supporting wake-vortex-free corridors for departing aircraft", Meteorological Applications, (May 2011)
9. Thomson, J. A. and S. M. Hannon. "Wake Vortex Modeling for Airborne and Ground Based Measurements Using A Coherent Lidar", Society of Photo-Optical Instrumentation Engineers (SPIE) Proceedings 2464, Orlando, FL, 1995: 63-78
10. F. Köpp et al., "Characterization of Aircraft Wake Vortices by 2-mm Pulsed Doppler Lidar", Journal of Atmospheric and Oceanic Technology 21, (2004): 194:206
11. S. Rahm and I. Smalikho. "Aircraft Wake Measurement with Airborne Coherent Doppler Lidar", Journal of Aircraft 45.4 (2008): 1148-1155.
12. P. Salamitou et al., "Simulation in the time domain for heterodyne coherent laser radar", Applied Optics, 34.3, (1999): 499-506,.
13. R. G. Frehlich and M. J. Kavaya, "Coherent Laser Radar Performance For General Atmospheric Refractive Turbulence", Applied Optics, 30, No. 36, 5325-5352, (1991).
14. V. A. Banakh and I. N. Smalikho, "Estimation of The Turbulence Energy Dissipation Rate From The Pulsed Doppler Lidar Data", Atmos. Oceanic Optics 10, No. 12, 957-965, (1997).

Appendix-A

a. Lidar Signal

The general form of the noisy complex Lidar signal at the receiver is.

$$\boldsymbol{z(t) = y(t) + n(t)} \quad \text{(A1)}$$

Where $y(t)$ the complex heterodyne signal. This signal is a function of the target properties, atmospheric parameter, and Lidar optical components. $n(t)$ is the additive shot noise at the photo-detector. The ensemble autocorrelation function (ACF) has the following form.

$$B_z(t, t+\tau) = B_y(t, t+\tau) + N.\delta_\tau \quad \text{(A2)}$$

$B_y(\tau)$ is ensemble ACF of the heterodyned signal component, N is the average noise power, and δ_τ is the Dirac delta function.

For stationary random processes the ensemble autocorrelation function (ACF) is theoretically equivalent to the time power ACF. The Fourier Transform of this power ACF yields the Power Spectral Density (PSD).

b. The time autocorrelation function

Starting from the time domain model of the complex heterodyne signal y(t)[12,13,14], the corresponding ensemble ACF can be found

$$B_y(t, t+\tau) = E\{y(t).y^*(t+\tau)\} = \quad \text{(A3)}$$

$$\frac{S(z_o)}{c}.\int_{-\infty}^{\infty} A_L\left(t - \frac{2.z}{c}\right) A^*{}_L\left(t - \frac{2.z}{c} + \tau\right) e^{i.\tau.\left(2\pi\Delta f + \frac{4\pi}{\lambda}V_r(z)\right)} dz$$

z_o is the radial distance to the center of the probing volume. $S(z_o)$ is the average heterodyne signal power assumed constant over the length of the probing volume. For the case of a Gaussian pulse

$$A_L(t) = \frac{1}{(2\pi\sigma^2)^{\frac{1}{4}}} e^{-\frac{\frac{1}{4}t^2}{\sigma^2}} \quad \text{(A4)}$$

The ensemble autocorrelation function becomes

$$B_y(t, t+\tau) = \frac{S(z_o)}{c}. \quad \text{(A5)}$$

$$\int_{-\infty}^{\infty} \frac{1}{\sqrt{2\pi}.\sigma} e^{-\frac{\left(t-\frac{2z}{c}-\frac{\tau}{2}\right)^2}{2\sigma^2}} . e^{-\frac{\tau^2}{8.\sigma^2}} . e^{i.\tau.\left(2\pi\Delta f + \frac{4\pi}{\lambda}V_r(z)\right)} dz$$

This is clearly a function of time and the signal is therefore non-stationary. However, for a small analysis time interval T centred at $2z_0/c$, the signal can be assumed to be locally stationary. Therefore the approximate ensemble ACF can be estimated using the time power ACF.

$$B_y(t, t+\tau) \sim B_y(\tau) = < y(t).y^*(t+\tau) >_T =$$

$$S(z_o).\int_{-\infty}^{\infty} \left(\frac{1}{cT} \int_{\frac{2z_0}{c}+\frac{\tau}{2}-\frac{T}{2}}^{\frac{2z_0}{c}+\frac{\tau}{2}+\frac{T}{2}} \frac{1}{\sqrt{2\pi}.\sigma} e^{-\frac{\left(t-\frac{2z}{c}+\frac{\tau}{2}\right)^2}{2\sigma^2}} . dt \right) \quad \text{(A6)}$$

$$e^{-\frac{\tau^2}{8.\sigma^2}} e^{i.\tau.\left(2\pi\Delta f + \frac{4\pi}{\lambda}V_r(z)\right)} . dz$$

$<.>_T$ represents the time average over the the analysis time interval T_A. The integral over time in parenthesis can be calculated by using a change of variable and the properties of the Error Function.

$$Q(z) = \frac{1}{cT}\left\{\operatorname{erf}\left(2\frac{z_0-z}{\sqrt{2}c\sigma}+\frac{T}{2\sqrt{2}\sigma}\right)-\operatorname{erf}\left(2\frac{z_0-z}{\sqrt{2}c\sigma}-\frac{T}{2\sqrt{2}\sigma}\right)\right\} \quad \text{(A7)}$$

Substituting (A7) back in equation (A6) results in the final form of the ACF.

$$B_y(\tau) = S(z_o).\int_{-\infty}^{\infty} Q(z).e^{-\frac{\tau^2}{8.\sigma^2}} e^{i.\tau.\left(2\pi\Delta f+\frac{4\pi}{\lambda}V_r(z)\right)}.dz \quad \text{(A8)}$$

Q(z) defines the spatial extent of the pulse or range gate resolution. It increases with both the analysis time interval and pulse duration.

c. Spectral Model

Taking the Fourier Transform of $B_z(\tau)$ leads to the desired PSD of the heterodyned signal.

$$S_y(f) = F\{B_y(\tau)\} = S(z_o).2.\sqrt{2\pi}\,\sigma \int_{-\infty}^{\infty} Q(z).e^{-2\sigma^2\left(2\pi\left(f-\Delta f+\frac{2}{\lambda}V_r(z)\right)\right)^2}.dz \quad \text{(A9)}$$

Assuming no mismatch in frequency between the LO and transmit pulse $\Delta f = 0$. The normalized spectrum of the total Lidar Signal is then found by taking the Fourier transform of (A2) and substituting for $S_y(f)$ using (A9) and dividing by N.

$$S_{nz}(f) = B.SNR(z_o)\int_{-\infty}^{\infty} Q'(z).e^{-\frac{1}{2}\frac{\left(f+\frac{2}{\lambda}V_r(z)\right)^2}{\sigma_f^2}}dz + 1 \quad \text{(A10)}$$

With $Q'(z) = 2.\sqrt{2\pi}\,\sigma.Q(z)$, $\sigma_f = \frac{1}{4\pi\sigma}$, and $SNR(z_o)=S(z_o)/(N.B)$. Where B represents the analog filter's bandwidth. Furthermore, since the spectrum is estimated using an FFT window of size T will broaden the spectrum. The resulting spectrum

$$\hat{S}_{nz}(f) = B.SNR(z_o)\int_{-\infty}^{\infty} Q'^{(z).e^{-\frac{1}{2}\frac{\left(f+\frac{2}{\lambda}V_r(z)\right)^2}{\sigma_{fb}^2}}}dz + 1 \quad \text{(A11)}$$

With $\sigma_{fb} = \sqrt{\sigma_f^2+\left(\frac{1}{3T}\right)^2}$